Journal of Alloys and Compounds 509 (2011) 8211–8214

Contents lists available at ScienceDirect

Journal of Alloys and Compounds

journal homepage: www.elsevier.com/locate/jallcom

Design of mesostructured γ-Fe_2O_3/carbon nanocomposites for electromagnetic wave absorption applications

Jianhua Zhou[a,b,*], Jianping He[a], Tao Wang[a], Guoxian Li[a], Yunxia Guo[a], Jianqing Zhao[a], Yiou Ma[a]

[a] College of Material Science and Technology, Nanjing University of Aeronautics and Astronautics, Nanjing 210016, China
[b] Key Laboratory of Renewable Energy and Gas Hydrate, Guangzhou Institute of Energy Conversion, Chinese Academy of Sciences, Guangzhou 510640, China

ARTICLE INFO

Article history:
Received 31 March 2011
Received in revised form 11 May 2011
Accepted 12 May 2011
Available online 19 May 2011

Keywords:
Mesostructure
Microwave absorption
Impedance matching
Magnetic properties

ABSTRACT

We propose and demonstrate a scheme to enhance microwave absorption property through mesoporous structure with high regularity. The mesostructured nanocomposites, embedding γ-Fe_2O_3 within carbon matrix, exhibit a strong and broadband attenuation of microwave in the frequency range of 0.5–18 GHz, mainly due to the better impedance matching. C-2Fe-900 exhibits strong absorption characteristics with an absorption peak of −32.0 dB at 6.4 GHz. The absorption peak intensity and position can be adjusted by changing the matching thickness of the coating. Reflection loss below −10 dB (i.e., absorption above 90%) is obtained in the frequency range of 1.9–10.7 GHz.

1. Introduction

Electromagnetic wave absorption materials are in high demand for both civil and military targets due to the increasing electromagnetic interference pollution [1,2]. Recently, the development of carbon-based materials with designed pore architecture may provide the possibility of a promising candidate for microwave absorbers, especially in the cases of light weight and harsh environment [3–7]. Their unique structure and properties can be utilized to overcome the shortcomings of conventional microwave absorbing materials [8–13]. Ordered mesoporous carbon CMK-3 embedded in mesoporous silica SBA-15 are built for electromagnetic interference shielding materials in the X band [14]. It was found that the unique mesostructure in the mesoporous carbon/fused silica composites largely favors microwave absorption. Furthermore, template strategy to prepare mesoporous carbon allows easily tuning the chemical component of framework in a very wide range. By simply adding inorganic salt, multifunctional hybrid mesoporous carbons have been synthesized via a solvent-evaporation induced self-assembly (EISA) approach [15,16]. In particular, ordered mesostructures with high metal content and dispersion can be obtained using metal citrate complex as precursor [17,18].

The purpose of this study was to demonstrate the effect of ordered mesoporous structure on the dissipation of electromagnetic wave in the frequency range of 0.5–18 GHz. Mesostructured γ-Fe_2O_3/carbon nanocomposites prepared with different contents and carbonization temperatures were investigated. It is found that the combination of ordered mesoporous structure and incorporation of magnetic species contribute to the better impedance matching, which results in the improved microwave absorption in a wide band.

2. Experimental

2.1. Materials

Poly(propylene oxide)-block-poly(ethylene oxide)-block-poly(propylene oxide) triblock copolymer Pluronic F127 (M_w = 12 600, $PEO_{106}PPO_{70}PEO_{106}$) was purchased from Sigma–Aldrich. Phenol, formaldehyde solution (37 wt%), ethanol, ferric citrate, and NaOH were purchased from Sinopharm Chemical Reagent Co., Ltd. All chemicals were used as received without any further purification. Millipore water was used in all experiments.

2.2. Synthesis

Ordered mesoporous γ-Fe_2O_3/C nanocomposites were prepared by a simple EISA route, where triblock copolymer F127 was used as a structure-directing agent, ferric citrate as a metal precursor, and resol as a carbon precursor [18]. According to the solvent evaporation, the concentration of F127 in the sol begins to exceed its critical micelle concentration, and the self-assembly of precursors is triggered at the same time. In a typical run, the carbon source (a low-molecular-weight phenol-formaldehyde resin [15]) was primarily prepared according to the previous report. Subsequently, F127 (1.0 g) was poured into ethanol (20.0 g) with vigorous stirring to obtain a clear solution. Ferric citrate solution (20 mL) and the carbon source (5.0 g, 20 wt% in ethanol) were added in succession. After stirring for 30 min, a homoge-

* Corresponding author at: Key Laboratory of Renewable Energy and Gas Hydrate, Guangzhou Institute of Energy Conversion, Chinese Academy of Sciences, Guangzhou 510640, China. Tel.: +86 20 87057592; fax: +86 20 87035351.
E-mail address: huajian0921@yahoo.com.cn (J. Zhou).

0925-8388/$ – see front matter © 2011 Elsevier B.V. All rights reserved.
doi:10.1016/j.jallcom.2011.05.042

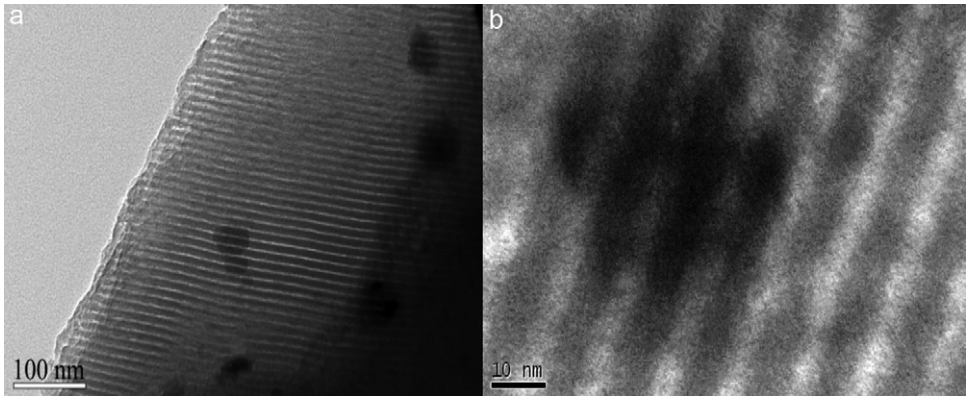

Fig. 1. TEM images for C-2Fe-700.

neous solution was obtained. The solution was transferred into dishes to evaporate ethanol at room temperature and then thermopolymerized in an oven at 100 °C for 24 h. The carbonization was carried out under N_2 atmosphere using always a heating rate of 1 °C min^{-1}. The resulting nanocomposites are denoted as C-*x*Fe-*y*, where *x* and *y* represent the content (×0.5 mmol) of ferric citrate added initially and the final temperature (°C) of carbonization, respectively.

2.3. Characterization

The samples were characterized by transmission electron microscopy (TEM, FEI Technai G^2) and X-ray powder diffraction (XRD, Bruker D8 Advance diffractometer with Cu Kα source). Hysteresis loops were measured by a vibrating sample magnetometer (Lakeshore VSM-7407) at room temperature.

For the studies of microwave absorption properties by using coaxial reflection/transmission technique, the prepared powder was dispersed in commercial epoxy resin which was used as binder matrix (the weight ratio of the prepared powder was about 40%), and then the mixture was pressed into toroid with outer diameter of 7.0 mm and inner diameter of 3.04 mm. The complex relative dielectric permittivity and magnetic permeability were obtained over 0.5–18 GHz using a vector network analyzer (Agilent E8363A). Reflection loss of powder–resin composites can be calculated using the measured dielectric permittivity and magnetic permeability according to transmission line theory.

3. Results and discussion

Fig. 1 reveals the mesoporous structure by TEM. It can be clearly seen that a parallel bands-like pore channels are highly arranged in the 1 1 0 direction, indicating a large region of ordered mesopores in the nanocomposites C-2Fe-700 (Fig. 1a). TEM image also shows high dispersion of small and uniform dark spots that correspond to iron oxide nanoparticles, which endows mesoporous carbon with a magnetic property [19]. The high-resolution TEM image, as shown in Fig. 1b, clearly indicates that an iron oxide nanoparticle with 40 nm in diameter incorporates in the ordered mesoporous structure, while the framework is poorly crystallized.

Supporting the TEM results, small-angle XRD pattern (Fig. 2a) of C-2Fe-700 shows a well-resolved diffraction peak around 2θ angle of 0.9°, which belongs to a typical ordered mesostructure. Wide-angle XRD pattern (Fig. 2b) of the mesostructured nanocomposites pyrolyzed at 700 °C present six resolved diffraction peaks. All the peaks are assigned to maghemite γ-Fe_2O_3 (JCPDS card 89-5892). In this mesostructure, the high porosity would decrease the bulk density of the prepared powder undoubtedly, making it possible to design a lighter and thinner electromagnetic wave absorber.

The electromagnetic parameters were measured over 0.5–18 GHz. Fig. 3a shows the imaginary part (ε) of the complex relative permittivity of the powder–resin composites. After heat treatment at 700 °C, the ε has a slight increase. The trends of permittivity with frequency are similar for the samples with increasing Fe content. For the sample just heat-treated at 500 °C, the ε of C-2Fe-500 is relatively low, indicating very poor dielectric loss. As the pyrolysis temperature increases, the complex permittivity of C-2Fe-900 becomes the largest one. It is noteworthy that there is a resonance peak around 5–14 GHz in the curves of ε. It reaches a maximum of 7.0 at 12.3 GHz, indicating that a higher level of graphitization would greatly enhance the dielectric loss. As we know, ε is related to electrical conductivity σ by the relation [20],

$$\varepsilon = \frac{\sigma}{2\pi f \varepsilon_0} \quad (1)$$

where ε_0 is the permittivity of free space and f is the frequency. The dielectric loss is enhanced through the raising carbonization temperature, which yields the semi-graphitic nature and in turn the high conductivity. Therefore, the main contribution for the high dielectric loss is the conductance loss and the dipole relaxation loss [21] in the γ-Fe_2O_3/carbon coupled objects.

The imaginary part (μ) of the complex relative permeability versus frequency is shown in Fig. 3b. A resonance peak around 3 GHz appears in the curves of μ. This nanocomposite with isolated magnetic particles possesses high surface area and large porosity, thus its surface anisotropy energy would be remarkably increased [22]. It leads to an increase of the effective anisotropy field and the shift to gigahertz region of the resonance frequency compared to sintered ferrite [23,24]. Interestingly, it is found that the μ values are negative, and the minimum value is up to −0.46 at 12.7 GHz for C-2Fe-900. Moreover, this trough is corresponding to the resonance peak of the imaginary permittivity, which is consistent with the phenomenon of the porous Fe_3O_4/SnO_2 core-shell nanorods [9] and Co nanochains [25]. It may be regarded as the radiation of magnetic energy [26]. As mentioned above, the conductivity of the nanocomposites pyrolyzed at 900 °C are enhanced. When they experience a changing electromagnetic field, the Lorentz force on

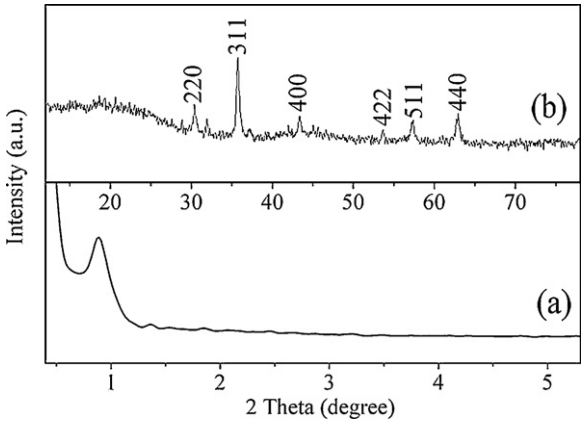

Fig. 2. Small-angle XRD (a) and wide-angle XRD (b) pattern for C-2Fe-700.

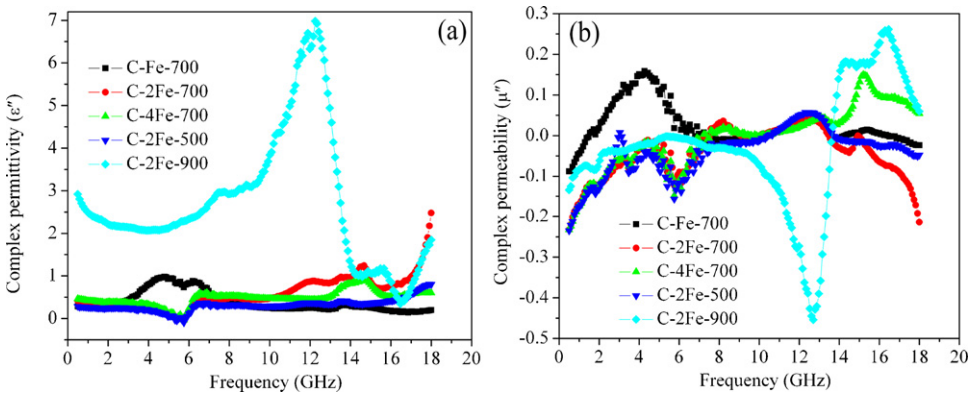

Fig. 3. Frequency dependences of imaginary part of (a) complex relative permittivity and (b) permeability of the nanocomposites.

electrons causes them to circulate around, forming eddy currents. The eddy currents then produce an induced magnetic field, which opposes the applied field. Energy is then radiated out. The eddy current loss can be written by the following expression [27–29].

$$f^{-1}(\mu')^{-2}\mu'' \approx \frac{2\pi\mu_0\sigma d^2}{3} \quad (2)$$

where μ_0 is the permeability of free space. If the magnetic loss results from eddy current loss, the values of $f^{-1}(\mu)^{-2}\mu$ should be a constant when the frequency is varied. As shown in Fig. 4, the values of $f^{-1}(\mu)^{-2}\mu$ increase by 0.20 in 0.5–4 GHz. Therefore, the natural resonance is dominant in the low frequencies and the corresponding resonance peaks are around 3 GHz. Additionally, the values have a little change over 4–18 GHz. The magnetic loss is mainly caused by eddy current loss in the high frequencies. Thus it can increase ε and lead a negative μ.

To investigate the static magnetic property of the nanocomposites, hysteresis loops are shown in Fig. 5. The saturation magnetization of the γ-Fe_2O_3/C nanocomposites is found to increase from 2.1 to 15.8 emu/g with the increase of Fe content and pyrolysis temperature, respectively. The values are much lower than that of the bulk γ-Fe_2O_3 (83 emu/g) [18], mainly due to a low content of γ-Fe_2O_3 (<15%) in the nanocomposites. The coercivity of the nanocomposites is ranging from 41 to 123 Oe, which suggests that there is an increase for effective anisotropy field of these nanocomposites comparing with that of the bulk γ-Fe_2O_3 or α-Fe [22]. Furthermore, the introduction of Fe species endows mesoporous carbon with a magnetic property, which would facilitate the balance of impedance matching.

On the basis of the previously measured electromagnetic parameters, reflection loss (R) of powder–resin composites can be obtained by calculation and simulation according to transmission line theory [30–32]. It is calculated as follows [13,33]:

$$Z_{in} = \sqrt{\frac{\mu_r}{\varepsilon_r}}\tanh\left[j\frac{2\pi fd}{c}\sqrt{\mu_r\varepsilon_r}\right] \quad (3)$$

$$R = 20\log\left|\frac{Z_{in}-1}{Z_{in}+1}\right| \quad (4)$$

where μ_r and ε_r are the complex relative magnetic permeability and dielectric permittivity of the composite medium, respectively, c is the velocity of electromagnetic waves in free space, f is the frequency of microwaves, and d is the thickness of an absorber.

Fig. 6a is the calculated reflection loss of the nanocomposites at the matching thickness of 3 mm. C-Fe-700 powder shows maximum reflection loss of only −4.8 dB and there is no absorption ranges under −10 dB. The effective absorption bandwidth, which is lower than −10 dB is 4.3 and 2.9 GHz as Fe content increases. For C-2Fe-900, it exhibits strong absorption characteristics with an absorption peak of −32.0 dB at 6.4 GHz. Fig. 6b shows a typical relationship between reflection loss and frequency for C-2Fe-900 at different thickness. The absorption peak shifts to a low frequency along with the increasing thickness. It exhibits microwave absorption bands could cover 1.9–10.7 GHz when adjusting the thicknesses from 2 to 9 mm. The behavior is important because it reveals that absorption peak frequency of the nanocomposites can be tuned easily by changing the matching thickness. The matching thickness can be optimized according to the needs. Additionally, it can be seen that the coupling of dielectric loss and magnetic loss

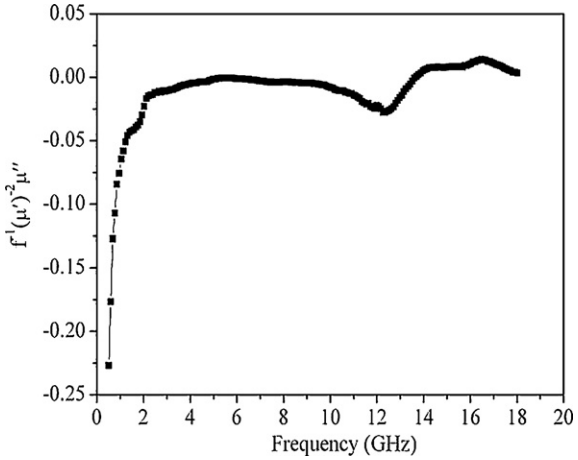

Fig. 4. Values $f^{-1}(\mu)^{-2}\mu$ of as a function of frequency for C-2Fe-900.

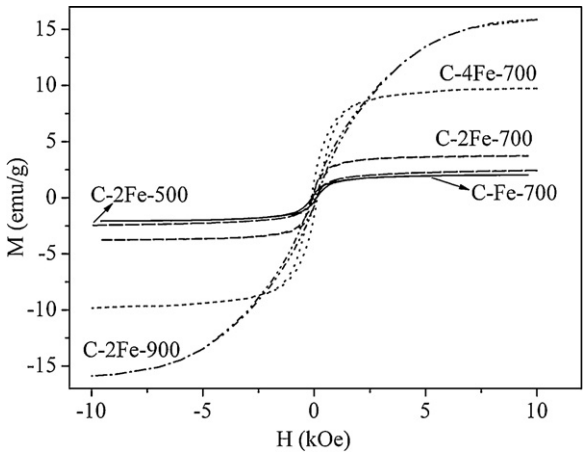

Fig. 5. Magnetic hysteresis loops at 300 K of the nanocomposites.

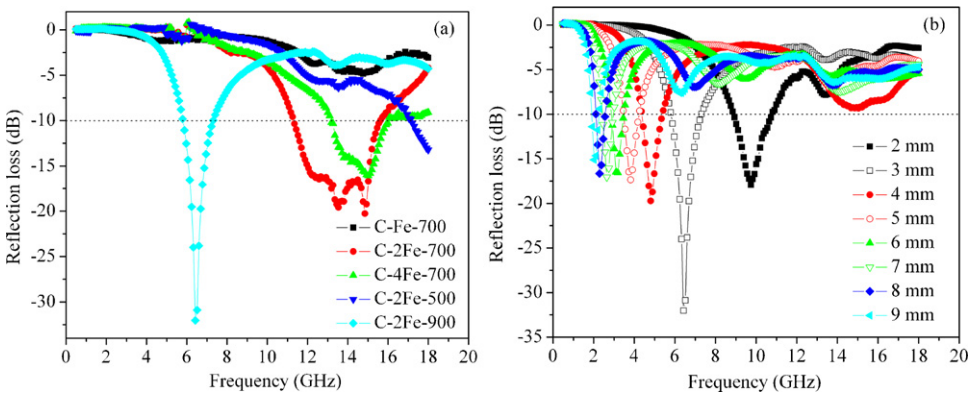

Fig. 6. Frequency–reflection curves of (a) the nanocomposites with a matching thickness of 3 mm and (b) C-2Fe-900 for different matching thicknesses.

contributes the reflection loss [13], due to the better impedance matching. For carbon materials, it is highly efficient for incorporating magnetic constituent to achieve a better impedance matching [34]. In this way, the electromagnetic wave can easily propagate within the absorber rather than directly reflect on the surface. Furthermore, electromagnetic wave could transmit through the mesoporous structure and generate the energy dissipation in many sites. This allows a sufficient absorption from all directions in the robust mesostructure.

4. Conclusions

Mesoporous γ-Fe_2O_3/C nanocomposites were prepared to realize a nanoscale impedance matching. The key feature of this method is the introduction of ferric citrate. At high carbonization temperature, the ordered mesostructure can ensure a fast and sufficient absorption of microwave. This material offers high corrosion resistance, lightweight and wide-frequency attenuation for use as multifunctional camouflage coatings.

Acknowledgements

This work was supported by Natural Science Foundation (50871053) and Aeronautical Science Foundation of China (2007ZF52061).

References

[1] R.C. Che, C.Y. Zhi, C.Y. Liang, X.G. Zhou, Appl. Phys. Lett. 88 (2006) 033105.
[2] R.C. Che, L.M. Peng, X.F. Duan, Q. Chen, X.L. Liang, Adv. Mater. 16 (2004) 401.
[3] A. Stein, Z.Y. Wang, M.A. Fierke, Adv. Mater. 21 (2009) 265.
[4] X.C. Gui, W. Ye, J.Q. Wei, K.L. Wang, R.T. Lv, H.W. Zhu, F.Y. Kang, J.L. Gu, D.H. Wu, J. Phys. D: Appl. Phys. 42 (2009) 075002.
[5] W.L. Song, M.S. Cao, Z.L. Hou, X.Y. Fang, X.L. Shi, J. Yuan, Appl. Phys. Lett. 94 (2009) 233110.
[6] W.L. Song, M.S. Cao, Z.L. Hou, J. Yuan, X.Y. Fang, Scripta Mater. 61 (2009) 201.
[7] M.S. Cao, W.L. Song, Z.L. Hou, B. Wen, J. Yuan, Carbon 48 (2010) 788.
[8] X. Tang, Q. Tian, B.Y. Zhao, K. Hu, Mater. Sci. Eng. A 35 (2007) 445–446.
[9] Y.J. Chen, P. Gao, R.X. Wang, C.L. Zhu, L.J. Wang, M.S. Cao, H.B. Jin, J. Phys. Chem. C 113 (2009) 10061.
[10] Q.L. Liu, D. Zhang, T.X. Fan, Appl. Phys. Lett. 93 (2008) 013110.
[11] G.X. Tong, W.H. Wu, J.G. Guan, H.S. Qian, J.H. Yuan, W. Li, J. Alloys Compd. 509 (2011) 4320.
[12] Y.Q. Kang, M.S. Cao, J. Yuan, L. Zhang, B. Wen, X.Y. Fang, J. Alloys Compd. 495 (2010) 254.
[13] S.B. Ni, X.H. Wang, G. Zhou, F. Yang, J.M. Wang, D.Y. He, J. Alloys Compd. 489 (2010) 252.
[14] J.C. Wang, C.S. Xiang, Q. Liu, Y.B. Pan, J.K. Guo, Adv. Funct. Mater. 18 (2008) 2995.
[15] R.L. Liu, Y.F. Shi, Y. Wan, Y. Meng, F.Q. Zhang, D. Gu, Z.X. Chen, B. Tu, D.Y. Zhao, J. Am. Chem. Soc. 128 (2006) 11652.
[16] J.H. Zhou, J.P. He, T. Wang, D. Sun, G.W. Zhao, X. Chen, D.J. Wang, Z.Y. Di, J. Mater. Chem. 18 (2008) 5776.
[17] T. Yu, Y.H. Deng, L. Wang, R.L. Liu, L.J. Zhang, B. Tu, D.Y. Zhao, Adv. Mater. 19 (2007) 2301.
[18] Y.P. Zhai, Y.Q. Dou, X.X. Liu, B. Tu, D.Y. Zhao, J. Mater. Chem. 19 (2009) 3292.
[19] I.S. Park, M. Choi, T.W. Kim, R. Ryoo, J. Mater. Chem. 19 (2006) 3409.
[20] T.N. Narayanan, V. Sunny, M.M. Shaijumon, P.M. Ajayan, M.R. Anantharaman, Electrochem. Solid-State Lett. 12 (2009) K21.
[21] X.G. Liu, D.Y. Geng, H. Meng, P.J. Shang, Z.D. Zhang, Appl. Phys. Lett. 92 (2008) 173117.
[22] X.L. Shi, M.S. Cao, J. Yuan, Q.L. Zhao, Y.Q. Kang, X.Y. Fang, Y.J. Chen, Appl. Phys. Lett. 93 (2008) 183118.
[23] E.S. Gorkunov, V.A. Zakharov, A.I. Ulyanov, A.A. Chulkina, Russ. J. Nondestruct. Test 37 (2001) 186.
[24] Y. Yang, B.S. Zhang, W.D. Xu, Y.B. Shi, Z.S. Jiang, N.S. Zhou, B.X. Gu, H.X. Lu, J. Magn. Magn. Mater. 256 (2003) 129.
[25] X.L. Shi, M.S. Cao, J. Yuan, X.Y. Fang, Appl. Phys. Lett. 95 (2009) 163108.
[26] L.J. Deng, M.G. Han, Appl. Phys. Lett. 91 (2007) 023119.
[27] M.Z. Wu, Y.D. Zhang, S. Hui, T.D. Xiao, S.H. Ge, W.A. Hines, J.I. Budnick, G.W. Taylor, Appl. Phys. Lett. 80 (2002) 4404.
[28] X.F. Zhang, X.L. Dong, H. Huang, Y.Y. Liu, W.N. Wang, X.G. Zhu, B. Lv, J.P. Lei, C.G. Lee, Appl. Phys. Lett. 89 (2006) 053115.
[29] X.G. Liu, J.J. Jiang, D.Y. Geng, B.Q. Li, Z. Han, W. Liu, Z.D. Zhang, Appl. Phys. Lett. 94 (2009) 053119.
[30] E. Michielssen, J. Sajer, S. Ranjithan, R. Mittra, IEEE Trans. Microwave Theory Tech. 41 (1993) 1024.
[31] M.S. Cao, J. Yuan, H.T. Liu, X.Y. Fang, J. Zhu, Mater. Design 24 (2003) 31.
[32] M.S. Cao, R.R. Qin, C.J. Qiu, J. Zhu, Mater. Design 24 (2003) 391.
[33] J.H. Zhou, J.P. He, G.X. Li, T. Wang, D. Sun, X.C. Ding, J.Q. Zhao, S.C. Wu, J. Phys. Chem. C 114 (2010) 7611.
[34] Q.L. Liu, D. Zhang, T.X. Fan, J.J. Gu, Y. Miyamoto, Z.X. Chen, Carbon 46 (2008) 461.